

# High-Order Spline Upwind for Space-Time Isogeometric Analysis

G. Loli<sup>1</sup>, G. Sangalli<sup>1,2</sup> and P. Tesini<sup>3,1</sup>

<sup>1</sup> Università di Pavia, Dipartimento di Matematica “F. Casorati”  
Via A. Ferrata 5, 27100 Pavia, Italy.  
{gabriele.loli, giancarlo.sangalli}@unipv.it

<sup>2</sup> IMATI-CNR “Enrico Magenes”, Pavia, Italy.

<sup>3</sup> Università degli Studi di Milano-Bicocca  
Piazza dell’Ateneo Nuovo 1, 20126 Milano, Italy.  
p.tesini@campus.unimib.it

## Abstract

We propose an innovative isogeometric space-time method for the heat equation, with smooth splines approximation in both space and time. To enhance the stability of the method we add a stabilizing term, based on a linear combination of high-order artificial diffusions. This term is designed in order to make the linear system lower block-triangular, that is, lower triangular with respect to time. In order to keep optimal accuracy, the stabilization terms are further weighted in terms of the residual. Through a series of numerical experiments, we validate the method’s capability, showcasing its stability and accuracy.

**Keywords:** Isogeometric Analysis, heat equation, space-time, splines, Upwind, SUPG

## 1 Introduction

Isogeometric Analysis (IgA), introduced in [1] (see also the book [2]), is an evolution of the classical finite element method. IgA uses spline functions, or their generalizations, both to represent the computational domain and to approximate the solution of the partial differential equation that models the problem of interest, in order to facilitate the interoperability between computer aided design (CAD) and numerical simulation. At the same time, IgA benefits from the properties of smooth splines, such as higher accuracy when compared to  $C^0$  piecewise polynomials (see e.g. [3, 4]).

The idea of using finite elements in the space-time domain comes from [5, 6, 7] and was then developed for various problems as heat transfer [8], advection-diffusion [9] and elastodynamics [10]. The mathematical theory of space-time Galerkin methods has been developed in recent works, for example [11, 12].

Space-time formulations in IgA provides an additional opportunity, that is, to exploit the properties of smooth splines in time as well, as proposed in [13, 14]. In particular, [14] develops a stabilized IgA of the heat equation. In [15, 16] the authors have proposed preconditioners and solvers, while in [17] a continuous space-time IgA formulation has been applied to linear and non-linear elastodynamics. The use of smooth splines with respect to time poses interesting challenges as well.

A challenge with space-time formulations concerns the causality principle. While the sequentiality of discontinuous Galerkin in time guarantees causality, this is not the case for Galerkin with smooth spline approximation in time. The lack of causality generates further unphysical behaviors in the case of numerical instability, as spurious oscillations may propagate backward in time.

Our aim in this paper is to design a Spline Upwind (SU) formulation of the heat equation, with a stabilization term that promotes causality. The proposed SU generalizes classical upwinding, as SUPG ([18]), to higher degree splines. We recall that SUPG method in time for the heat equation and with piecewise linear finite elements leads to a lower block-triangular linear system. Stability is further enhanced by adding artificial diffusion when the residual is higher, as with Shock Capturing. These techniques concomitantly promotes causality and stability, thereby enhancing the overall computational robustness. The proposed SU extends these ideas to higher degree splines. We first enrich the plain Galerkin formulation by diffusion terms of different order, such

that the resulting linear system is block triangular with respect to time. These terms are then weighted by the residual in order to preserve the optimal convergence rate when the solution is smooth.

We perform numerical tests to assess the expected behavior of the proposed SU formulation. In particular, motivated by the interest for space-time simulation of laser-based additive manufacturing (see [19]), we perform experiments with a concentrated source term, showing that the numerical solution is free from spurious oscillations.

While the focus of our work is not on computational cost, we also acknowledge that space-time formulations pose challenges in terms of their computational cost. The augmented dimensionality detrimentally impacts conventional solvers. However, it is noteworthy that space-time formulations hold promise for local mesh refinement [20] and parallelisation [21], attracting interest in the field, see also the recent book [22].

The outline of the paper is as follows. The basics of IgA are discussed in Section 2. In Section 3 we review some stabilized formulations in one dimension, for advection and advection-diffusion equations, and introduce the new SU formulation. In Section 4 we apply SU to the heat equation. We propose numerical tests, assessing the performance of the presented stabilizing methods, in Section 5. Finally, in the last section we draw conclusions and highlight some future research directions.

## 2 Preliminaries

We recall the notation and definitions of [16].

Given  $n$  and  $p$  two positive integers, we consider the knot vector

$$\widehat{\Xi} := \left\{ 0 = \widehat{\xi}_1 = \dots = \widehat{\xi}_{p+1} \leq \dots \leq \widehat{\xi}_n = \dots = \widehat{\xi}_{n+p+1} = 1 \right\}$$

and the vector  $\widehat{Z} := \{\widehat{\zeta}_1, \dots, \widehat{\zeta}_m\}$  of knots without repetitions (i.e. breakpoints).

The univariate spline space is defined as

$$\widehat{\mathcal{S}}_h^p := \text{span}\{\widehat{b}_{i,p}\}_{i=1}^n,$$

where  $\widehat{b}_{i,p}$  are the univariate B-splines and  $\widehat{h}$  denotes the mesh-size, i.e.  $\widehat{h} := \max\{|\widehat{\xi}_{i+1} - \widehat{\xi}_i| \text{ s.t. } i = 1, \dots, n+p\}$ . For more details on B-splines properties and their use in IgA we refer to [2].

Multivariate B-splines are tensor product of univariate B-splines. We consider functions that depend on  $d$  spatial variables and the time variable. Given positive integers  $n_l, p_l$  for  $l = 1, \dots, d$  and  $n_t, p_t$ , we define  $d+1$  univariate knot vectors  $\widehat{\Xi}_l := \{\widehat{\xi}_{l,1} \leq \dots \leq \widehat{\xi}_{l,n_l+p_l+1}\}$  for  $l = 1, \dots, d$  and  $\widehat{\Xi}_t := \{\widehat{\xi}_{t,1} \leq \dots \leq \widehat{\xi}_{t,n_t+p_t+1}\}$  and  $d+1$  breakpoints vectors  $\widehat{Z}_l := \{\widehat{\zeta}_{l,1}, \dots, \widehat{\zeta}_{l,m_l}\}$  for  $l = 1, \dots, d$  and  $\widehat{Z}_t := \{\widehat{\zeta}_{t,1}, \dots, \widehat{\zeta}_{t,m_t}\}$ . Let  $\widehat{h}_l$  be the mesh-size associated to the knot vector  $\widehat{\xi}_l$  for  $l = 1, \dots, d$ , let  $\widehat{h}_s := \max\{\widehat{h}_l \mid l = 1, \dots, d\}$  be the maximal mesh-size in all spatial knot vectors and let  $\widehat{h}_t$  be the mesh-size of the time knot vector.

Let also  $\mathbf{p}$  be the vector that contains the degree of each univariate spline space, i.e.  $\mathbf{p} := (\mathbf{p}_s, p_t)$ , where  $\mathbf{p}_s := (p_1, \dots, p_d)$ .

The multivariate B-splines are defined as

$$\widehat{B}_{\mathbf{i},\mathbf{p}}(\boldsymbol{\eta}, \tau) := \widehat{B}_{\mathbf{i}_s,\mathbf{p}_s}(\boldsymbol{\eta}) \widehat{b}_{i_t,p_t}(\tau),$$

where

$$\widehat{B}_{\mathbf{i}_s,\mathbf{p}_s}(\boldsymbol{\eta}) := \widehat{b}_{i_1,p_1}(\eta_1) \dots \widehat{b}_{i_d,p_d}(\eta_d),$$

$\mathbf{i}_s := (i_1, \dots, i_d)$ ,  $\mathbf{i} := (\mathbf{i}_s, i_t)$  and  $\boldsymbol{\eta} = (\eta_1, \dots, \eta_d)$ . The corresponding spline space is defined as

$$\widehat{\mathcal{S}}_h^{\mathbf{p}} := \text{span} \left\{ \widehat{B}_{\mathbf{i},\mathbf{p}} \mid i_l = 1, \dots, n_l \text{ for } l = 1, \dots, d; i_t = 1, \dots, n_t \right\},$$

and  $\widehat{h} := \max\{\widehat{h}_s, \widehat{h}_t\}$ . We have that  $\widehat{\mathcal{S}}_h^{\mathbf{p}} = \widehat{\mathcal{S}}_{h_s}^{\mathbf{p}_s} \otimes \widehat{\mathcal{S}}_{h_t}^{p_t}$ , where

$$\widehat{\mathcal{S}}_{h_s}^{\mathbf{p}_s} := \text{span} \left\{ \widehat{B}_{\mathbf{i}_s,\mathbf{p}_s} \mid i_l = 1, \dots, n_l; l = 1, \dots, d \right\}$$

is the space of tensor-product splines on  $\widehat{\Omega} := (0, 1)^d$ .

We assume that  $p_t, p_s \geq 1$  and that  $\widehat{\mathcal{S}}_{h_s}^{p_s} \subset C^0(\widehat{\Omega})$  and  $\widehat{\mathcal{S}}_{h_t}^{p_t} \subset C^{p_t-1}((0, 1))$ . We allow variable continuity in space since it may be useful for geometry representation, while we consider only maximum continuity with respect to time in order to benefit from the approximation properties of smooth splines, see [3, 4].

We denote by  $\Omega \times (0, T)$  the space-time computational domain, where  $\Omega \subset \mathbb{R}^d$  ( $d$  denotes the space dimension) and  $\Omega$  is parametrized by  $\mathbf{F} : \widehat{\Omega} \rightarrow \Omega$ , with  $\mathbf{F} \in \widehat{\mathcal{S}}_{h_s}^{p_s}$ , and  $T > 0$  is the final time. The space-time domain is parametrized by  $\mathbf{G} : \widehat{\Omega} \times (0, 1) \rightarrow \Omega \times (0, T)$ , such that  $\mathbf{G}(\boldsymbol{\eta}, \tau) := (\mathbf{F}(\boldsymbol{\eta}), T\tau) = (\mathbf{x}, t)$ .

The spline space with initial and boundary conditions, in parametric coordinates, is

$$\widehat{\mathcal{X}}_h := \left\{ \widehat{v}_h \in \widehat{\mathcal{S}}_h^p \mid \widehat{v}_h = 0 \text{ on } \partial\widehat{\Omega} \times (0, 1) \text{ and } \widehat{v}_h = 0 \text{ on } \widehat{\Omega} \times \{0\} \right\}.$$

We also have that  $\widehat{\mathcal{X}}_h = \widehat{\mathcal{X}}_{s, h_s} \otimes \widehat{\mathcal{X}}_{t, h_t}$ , where

$$\begin{aligned} \widehat{\mathcal{X}}_{s, h_s} &:= \left\{ \widehat{w}_h \in \widehat{\mathcal{S}}_{h_s}^{p_s} \mid \widehat{w}_h = 0 \text{ on } \partial\widehat{\Omega} \right\} \\ &= \text{span} \left\{ \widehat{b}_{i_1, p_s} \dots \widehat{b}_{i_d, p_s} \mid i_l = 2, \dots, n_l - 1; l = 1, \dots, d \right\}, \\ \widehat{\mathcal{X}}_{t, h_t} &:= \left\{ \widehat{w}_h \in \widehat{\mathcal{S}}_{h_t}^{p_t} \mid \widehat{w}_h(0) = 0 \right\} = \text{span} \left\{ \widehat{b}_{i_t, p_t} \mid i_t = 2, \dots, n_t \right\}. \end{aligned}$$

With a colexicographical reordering of the basis functions, we write

$$\begin{aligned} \widehat{\mathcal{X}}_{s, h_s} &= \text{span} \left\{ \widehat{b}_{i_1, p_s} \dots \widehat{b}_{i_d, p_s} \mid i_l = 1, \dots, n_{s,l}; l = 1, \dots, d \right\} \\ &= \text{span} \left\{ \widehat{B}_{i, p_s} \mid i = 1, \dots, N_s \right\}, \\ \widehat{\mathcal{X}}_{t, h_t} &= \text{span} \left\{ \widehat{b}_{i, p_t} \mid i = 1, \dots, N_t \right\}, \end{aligned}$$

and

$$\widehat{\mathcal{X}}_h = \text{span} \left\{ \widehat{B}_{i, p} \mid i = 1, \dots, N_{dof} \right\}, \quad (1)$$

where  $n_{s,l} := n_l - 2$  for  $l = 1, \dots, d$ ,  $N_s := \prod_{l=1}^d n_{s,l}$ ,  $N_t := n_t - 1$  and  $N_{dof} := N_s N_t$ .

Our isogeometric space is the isoparametric push-forward of (1) through the geometric map  $\mathbf{G}$ , i.e.

$$\mathcal{X}_h := \text{span} \left\{ B_{i, p} := \widehat{B}_{i, p} \circ \mathbf{G}^{-1} \mid i = 1, \dots, N_{dof} \right\},$$

where again  $\mathcal{X}_h = \mathcal{X}_{s, h_s} \otimes \mathcal{X}_{t, h_t}$ , with

$$\mathcal{X}_{s, h_s} := \text{span} \left\{ B_{i, p_s} := \widehat{B}_{i, p_s} \circ \mathbf{F}^{-1} \mid i = 1, \dots, N_s \right\}$$

and

$$\mathcal{X}_{t, h_t} := \text{span} \left\{ b_{i, p_t}(\cdot) := \widehat{b}_{i, p_t} \left( \frac{\cdot}{T} \right) \mid i = 1, \dots, N_t \right\}.$$

Moreover we define the breakpoints in the time interval as:

$$\zeta_{t,i} := T \widehat{\zeta}_{t,i} \quad \text{for } i = 1, \dots, m_t,$$

and the time steps as:

$$h_{t,i} := \zeta_{t,i+1} - \zeta_{t,i} \quad \text{for } i = 1, \dots, m_t - 1.$$

### 3 Upwinding in one dimension

Our first model problem is the unidimensional advection: we look for a function  $u$  such that

$$\begin{cases} u' &= f & \text{in } (0, T) \\ u(0) &= 0 \end{cases} \quad (2)$$

We assume that  $f \in L^2(0, T)$  and consider the following Galerkin method:

$$\text{find } u_h \in \mathcal{X}_{t, h_t} \text{ such that } \mathcal{A}(u_h; v_h) = \mathcal{F}(v_h) \quad \forall v_h \in \mathcal{X}_{t, h_t},$$

where

$$\mathcal{A}(u_h; v_h) := \int_0^T u_h' v_h \, dt \quad \text{and} \quad \mathcal{F}(v) := \int_0^T f v_h \, dt.$$

### 3.1 Standard Upwind and Shock Capturing

The Streamline Upwind Petrov Galerkin (SUPG) method, see [18], reads:

$$\text{find } u_h \in \mathcal{X}_{t,h_t} \text{ such that } \mathcal{A}(u_h; v_h) + \mathcal{S}_{\text{SUPG}}(u_h, f; v_h) = \mathcal{F}(v_h) \quad \forall v_h \in \mathcal{X}_{t,h_t}, \quad (3)$$

where

$$\mathcal{S}_{\text{SUPG}}(u_h, f; v_h) := \sum_{i=1}^{m_t-1} \tau_{\text{SUPG},i} \int_{\zeta_{t,i}}^{\zeta_{t,i+1}} (u'_h - f) v'_h \, dt,$$

In order to enhance the stability of SUPG, we can further add a Shock Capturing term leading to:

$$\text{find } u_h \in \mathcal{X}_{t,h_t} \text{ such that } \mathcal{A}(u_h; v_h) + \mathcal{S}_{\text{SUPG}}(u_h, f; v_h) + \mathcal{S}_{\text{SC}}(u_h; v_h) = \mathcal{F}(v_h) \quad \forall v_h \in \mathcal{X}_{t,h_t},$$

where, following [23],

$$\mathcal{S}_{\text{SC}}(u_h; v_h) := \sum_{i=1}^{m_t-1} \int_{\zeta_{t,i}}^{\zeta_{t,i+1}} \kappa_{\text{SC},i} u'_h v'_h \, dt \quad \text{and} \quad \kappa_{\text{SC},i} := \tau_{\text{SC},i} \frac{|u'_h - f|}{u_{\text{ref}}}, \quad \text{with } \tau_{\text{SC},i} := \frac{h_{t,i}^2}{4}$$

and  $u_{\text{ref}}$  is a reference magnitude for  $u_h$ .

### 3.2 High-order Upwind

With the choice  $\tau_{\text{SUPG},i} = \frac{h_{t,i}}{2}$  and when  $p_t = 1$ , formulation (3) leads to a lower triangular linear system. However, for higher degree splines, the matrix does not exhibit a lower triangular structure regardless of the  $\tau_{\text{SUPG},i}$  value chosen. This motivates the design of a new high-order Non-Consistent Spline Upwind (NCSU) formulation for spline with maximum continuity  $C^{p_t-1}$ :

$$\text{find } u_h \in \mathcal{X}_{t,h_t} \text{ such that } \mathcal{A}(u_h; v_h) + \mathcal{S}_{\text{NCSU}}(u_h; v_h) = \mathcal{F}(v_h) \quad \forall v_h \in \mathcal{X}_{t,h_t}, \quad (4)$$

where the new stabilizing term fulfils

$$\mathcal{S}_{\text{NCSU}}(u_h; v_h) := \sum_{k=1}^{p_t} \sum_{i=1}^{m_t-1} h_{t,i}^{2k-1} \int_{\zeta_{t,i}}^{\zeta_{t,i+1}} \tau_k(t) u_h^{(k)} v_h^{(k)} \, dt,$$

where each  $\tau_k(T \cdot) \in \widehat{\mathcal{S}}_{h_t}^{p_t-k} \in C^{p_t-k-1}$  is a spline with maximum continuity that is selected in order to make the linear system matrix lower triangular, that is:

$$\int_0^T b'_{\ell+i,p_t} b_{i,p_t} \, dt + \sum_{k=1}^{p_t} \sum_{j=1}^{m_t-1} h_{t,j}^{2k-1} \int_{\zeta_{t,j}}^{\zeta_{t,j+1}} \tau_k(t) b'_{\ell+i,p_t} b_{i,p_t}^{(k)} \, dt = 0, \quad (5)$$

for  $i = 1, \dots, N_t - 1$  and  $\ell = 1, \dots, r$ , with  $r = \min(p_t, N_t - i)$ .

In all our numerical tests we have observed that (5) is well posed and that the  $\tau_k$  are bounded; in particular the  $\tau_k$  are positive in most of the domain and where they are negative, they are much smaller in magnitude. In Figures 1 and 2 we have plotted  $\tau_k(t)$  for different degrees and meshes.

However, the formulation above is non consistent and lacks optimal convergence. To overcome this limitation we introduce a non-linear weighting based on residual denoted for brevity Spline Upwind (SU) method, and defined as:

$$\text{find } u_h \in \mathcal{X}_{t,h_t} \text{ such that } \mathcal{A}(u_h; v_h) + \mathcal{S}_{\text{SU},1}(u_h, f; v_h) + \mathcal{S}_{\text{SU},2}(u_h; v_h) = \mathcal{F}(v_h) \quad \forall v_h \in \mathcal{X}_{t,h_t}, \quad (6)$$

with

$$\mathcal{S}_{\text{SU},1}(u_h, f; v_h) := \sum_{i=1}^{m_t-1} h_{t,i} \int_{\zeta_{t,i}}^{\zeta_{t,i+1}} \tau_1(t) (u'_h - (1 - \theta(t))f) v'_h \, dt,$$

and

$$\mathcal{S}_{\text{SU},2}(u_h; v_h) := \sum_{k=2}^{p_t} \sum_{i=1}^{m_t-1} h_{t,i}^{2k-1} \int_{\zeta_{t,i}}^{\zeta_{t,i+1}} \tau_k(t) \theta(t) u_h^{(k)} v_h^{(k)} \, dt,$$

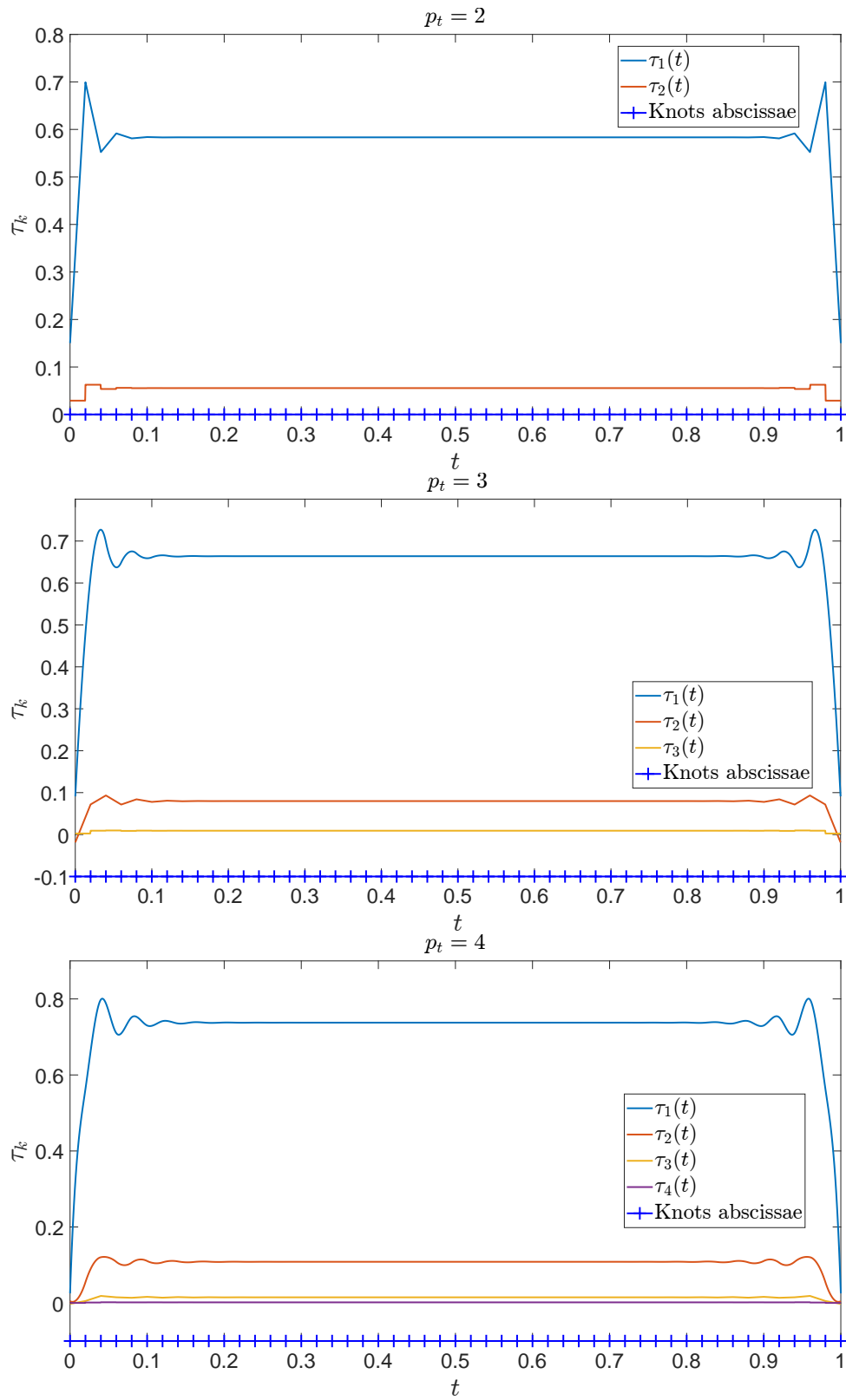


Figure 1: Plot of  $\tau_k(t)$  for uniform meshes, with  $h_t = 1/50$  and  $p_t = 2, 3, 4$ .

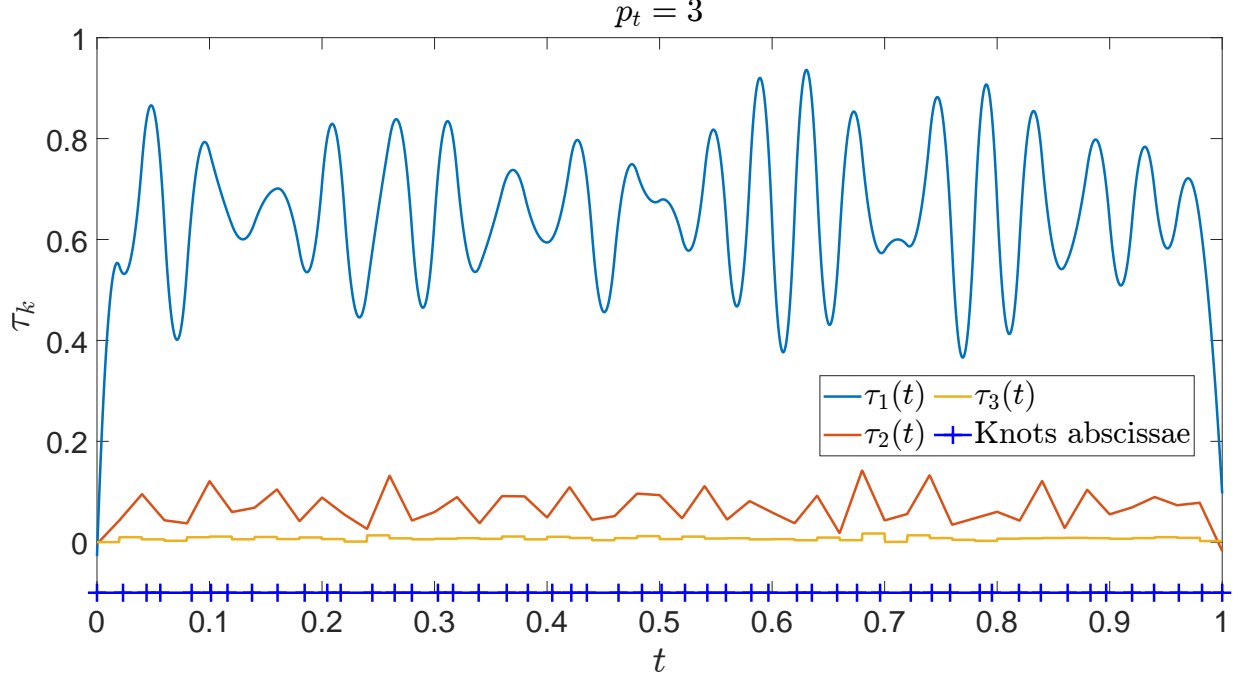


Figure 2: Plot of  $\tau_k(t)$  for a non-uniform mesh (the knots are represented by the blue vertical segments on the horizontal axis) and  $p_t = 3$ .

where  $\theta(t)$  is a piecewise linear interpolation of  $\theta_i$  computed in the breakpoints  $\zeta_{t,i}$  for  $i = 1, \dots, m_t$  as:

$$\theta_i := \min(\text{res}_i, 1),$$

with the relative residual  $\text{res}_i$  defined as

$$\text{res}_i := \frac{\|u'_h - f\|_{L^\infty([\zeta_{t,\max(1,i-1)}, \zeta_{t,\min(i+1, m_t)}])}}{T^{-1} \|u_h\|_{L^\infty([0, T])} + \|u'_h\|_{L^\infty([0, T])}}.$$

The definition of  $\theta$  is such that when the residual is high, e.g., within layers,  $\theta \approx 1$  and SU locally reduces to NCSU (4).

For advection-diffusion problem

$$\begin{cases} -\varepsilon u'' + u' = f & \text{in } (0, T) \\ u(0) = u(T) = 0 \end{cases} \quad (7)$$

where  $\varepsilon > 0$ , SU is extended straightforwardly by redefining  $\mathcal{S}_{\text{SU},1}$  in (6) as follows

$$\mathcal{S}_{\text{SU},1}(u_h, f; v_h) := \sum_{i=1}^{m_t-1} h_{t,i} \int_{\zeta_{t,i}}^{\zeta_{t,i+1}} \tau_1(t) (u'_h - (1 - \theta(t))(-\varepsilon u''_h - f)) v'_h \, dt,$$

and

$$\theta_i := \min(\text{res}_i, 1),$$

with

$$\text{res}_i := \frac{\|-\varepsilon u''_h + u'_h - f\|_{L^\infty([\zeta_{t,\max(1,i-1)}, \zeta_{t,\min(i+1, m_t)}])}}{T^{-1} \|u_h\|_{L^\infty([0, T])} + \|u'_h\|_{L^\infty([0, T])}}.$$

## 4 Upwinding the heat equation

Consider the heat equation with homogeneous boundary and initial condition

$$\begin{cases} \partial_t u - \Delta u = f & \text{in } \Omega \times (0, T) \\ u = 0 & \text{on } \partial\Omega \times [0, T] \\ u = 0 & \text{in } \Omega \times \{0\} \end{cases} \quad (8)$$

Introducing the bilinear form  $\mathcal{A}(\cdot; \cdot)$  and the linear form  $\mathcal{F}(\cdot)$  as

$$\mathcal{A}(w; v) := \int_0^T \int_{\Omega} (\partial_t w v + \nabla w \cdot \nabla v) \, d\Omega \, dt \quad \text{and} \quad \mathcal{F}(v) := \int_0^T \int_{\Omega} f v \, d\Omega \, dt$$

we consider the Galerkin method:

$$\text{find } u_h \in \mathcal{X}_h \text{ such that } \mathcal{A}(u_h; v_h) = \mathcal{F}(v_h) \quad \forall v_h \in \mathcal{X}_h.$$

The matrix of the linear system is

$$\mathbf{W}_t \otimes \mathbf{M}_s + \mathbf{M}_t \otimes \mathbf{K}_s, \quad (9)$$

where for  $i, j = 1, \dots, N_t$

$$[\mathbf{W}_t]_{i,j} = \int_0^T b'_{j,p_t}(t) b_{i,p_t}(t) \, dt \quad \text{and} \quad [\mathbf{M}_t]_{i,j} = \int_0^T b_{j,p_t}(t) b_{i,p_t}(t) \, dt,$$

while for  $i, j = 1, \dots, N_s$

$$[\mathbf{K}_s]_{i,j} = \int_{\Omega} \nabla B_{j,p_s}(\mathbf{x}) \cdot \nabla B_{i,p_s}(\mathbf{x}) \, d\Omega \quad \text{and} \quad [\mathbf{M}_s]_{i,j} = \int_{\Omega} B_{j,p_s}(\mathbf{x}) B_{i,p_s}(\mathbf{x}) \, d\Omega.$$

The SUPG method reads:

$$\text{find } u_h \in \mathcal{X}_h \text{ such that } \mathcal{A}(u_h; v_h) + \mathcal{S}_{\text{SUPG}}(u_h, f; v_h) = \mathcal{F}(v_h) \quad \forall v_h \in \mathcal{X}_h, \quad (11)$$

where

$$\mathcal{S}_{\text{SUPG}}(u_h, f; v_h) := \sum_{i=1}^{m_t-1} \tau_{\text{SUPG},i} \int_{\zeta_{t,i}}^{\zeta_{t,i+1}} \int_{\Omega} (\partial_t u_h - \Delta u_h - f) \partial_t v_h \, d\Omega \, dt.$$

With the choice  $\tau_{\text{SUPG},i} = \frac{h_{t,i}}{2}$  and when  $p_t = 1$ , formulation (11) lead to a lower block triangular time derivative matrix.

The new space-time formulation for the heat equation is based, as in the SU one-dimensional formulation, on the idea of modifying (9) in order to obtain lower triangular time matrices. This is accomplished by introducing numerical diffusion in the time direction. The proposed method reads:

$$\text{find } u_h \in \mathcal{X}_h \text{ such that } \mathcal{A}(u_h; v_h) + \mathcal{S}_{\text{SU},1}(u_h, f; v_h) + \mathcal{S}_{\text{SU},2}(u_h; v_h) + \mathcal{S}_{\text{SU},3}(u_h; v_h) = \mathcal{F}(v_h) \quad \forall v_h \in \mathcal{X}_h, \quad (12)$$

where for  $i, j = 1, \dots, N_{\text{dof}}$

$$\mathcal{S}_{\text{SU},1}(u_h, f; v_h) := \sum_{i=1}^{m_t-1} h_{t,i} \int_{\zeta_{t,i}}^{\zeta_{t,i+1}} \tau_1(t) \int_{\Omega} (\partial_t u_h + (1 - \theta(\mathbf{x}, t))(-\Delta u_h - f)) \partial_t v_h \, d\Omega \, dt,$$

and

$$\mathcal{S}_{\text{SU},2}(u_h; v_h) := \sum_{k=2}^{p_t} \sum_{i=1}^{m_t-1} h_{t,i}^{2k-1} \int_{\zeta_{t,i}}^{\zeta_{t,i+1}} \tau_k(t) \int_{\Omega} \theta(\mathbf{x}, t) \partial_t^k u_h \partial_t^k v_h \, d\Omega \, dt,$$

while

$$\mathcal{S}_{\text{SU},3}(u_h; v_h) := \sum_{k=1}^{p_t} \sum_{i=1}^{m_t-1} h_{t,i}^{2k} \int_{\zeta_{t,i}}^{\zeta_{t,i+1}} \sigma_k(t) \int_{\Omega} \theta(\mathbf{x}, t) (\nabla(\partial_t^k u_h) \cdot \nabla(\partial_t^k v_h)) \, d\Omega \, dt.$$

As in the Section 3.2,  $\tau_k(T \cdot) \in \widehat{\mathcal{S}}_{h_t}^{p_t-k}$  with maximum continuity, are selected such that:

$$\int_0^T b'_{\ell+i,p_t} b_{i,p_t} \, dt + \sum_{k=1}^{p_t} \sum_{j=1}^{m_t-1} h_{t,j}^{2k-1} \int_{\zeta_{t,j}}^{\zeta_{t,j+1}} \tau_k(t) b_{\ell+i,p_t}^{(k)} b_{i,p_t}^{(k)} \, dt = 0, \quad (13)$$

for  $i = 1, \dots, N_t - 1$  and  $\ell = 1, \dots, r$ , with  $r = \min(p_t, N_t - i)$ ,

while  $\sigma_k(T \cdot) \in \widehat{\mathcal{S}}_{h_t}^{p_t-k}$  with maximum continuity, are selected in order to make the time mass matrix lower triangular:

$$\int_0^T b_{\ell+i,p_t} b_{i,p_t} \, dt + \sum_{k=1}^{p_t} \sum_{j=1}^{m_t-1} h_{t,j}^{2k} \int_{\zeta_{t,j}}^{\zeta_{t,j+1}} \sigma_k(t) b_{\ell+i,p_t}^{(k)} b_{i,p_t}^{(k)} \, dt = 0, \quad (14)$$

for  $i = 1, \dots, N_t - 1$  and  $\ell = 1, \dots, r$ , with  $r = \min(p_t, N_t - i)$ .

The function  $\theta(\mathbf{x}, t)$  ranges from 0 to 1. If we set  $\theta$  as a fixed parameter equal to 1, (12) yields a block lower triangular global system matrix. However, in order to achieve optimal order of convergence, similar to the one-dimensional case (see Section 3.2), we define  $\theta(\mathbf{x}, t)$  as a piecewise  $(d + 1)$ -linear interpolation of  $\theta_{\mathbf{i}, j}$  computed in the breakpoints, where for  $\mathbf{i} = (i_1, \dots, i_d)$ ,  $i_l = 1, \dots, m_l$ ,  $l = 1, \dots, d$ , and  $j = 1, \dots, m_t$  we set

$$\theta_{\mathbf{i}, j} := \min(\text{res}_{\mathbf{i}, j}, 1),$$

with

$$\text{res}_{\mathbf{i}, j} := \frac{\|\partial_t u_h - \Delta u_h - f\|_{L^\infty(\psi_s \times \psi_t)}}{T^{-1} \|u_h\|_{L^\infty(\Omega \times [0, T])} + \|\partial_t u_h\|_{L^\infty(\Omega \times [0, T])}},$$

where

$$\psi_s = [\zeta_{1, \max(1, i_1 - 1)}, \zeta_{1, \min(i_1 + 1, m_1)}] \times \dots \times [\zeta_{d, \max(1, i_d - 1)}, \zeta_{d, \min(i_d + 1, m_d)}],$$

and

$$\psi_t = [\zeta_{t, \max(1, j - 1)}, \zeta_{t, \min(j + 1, m_t)}].$$

## 5 Numerical Results

In the following, all numerical tests are conducted using Matlab R2023a and the GeoPDEs toolbox [24]. Just for the sake of simplicity, in all our tests we consider splines of the same polynomial degree in all parametric directions for space and time. Specifically, we set  $p_1 = \dots = p_d = p_t := p$ . Additionally, although the proposed methods are designed for maximum regularity only with respect to time, we choose to use splines of global maximum continuity  $C^{p-1}$  also with respect to space. Numerical tests with different degrees and regularities (in space) indeed yield results entirely analogous to those reported below.

Nonlinearities in the equations are addressed through fixed point iterations, and the resulting linear systems are solved using the direct solver provided by Matlab.

We would like to emphasize that the main focus of this work is not on computational costs, and as such, we do not discuss or analyze the efficiency associated with the proposed method.

### 5.1 Advection equation

We consider the advection equation (2) on  $(0, T)$  with  $T = 1$  and uniform mesh.

#### 5.1.1 Smooth solution

We set  $f = 50 \cos(50t)$  such that the exact solution is  $u_{\text{ex}}(t) = \sin(50t)$ . In Figure 3, we show the error plot for the SU formulation on uniform meshes and degree  $p = 1, \dots, 6$  and we see that the method is optimally convergent.

#### 5.1.2 Solution with layers

We select  $f$  such that the exact solution is

$$u_{\text{ex}}(t) = \sin(50t) + 10 \frac{1 + \tanh(\frac{t-t_0}{\delta})}{2} - 5 \frac{1 + \tanh(\frac{t-t_1}{\delta})}{2} - 5 \frac{1 + \tanh(\frac{t-t_2}{\delta})}{2},$$

with  $t_0 = 0.3$ ,  $t_1 = 0.5$ ,  $t_2 = 0.7$  and  $\delta = 10^{-3}$ . Also on uniform meshes, due to the presence of internal layers, the standard Galerkin solution is unstable (see Figure 4). For high-degree splines, plain SUPG has spurious oscillations, for any value of the stability parameter  $\tau_{\text{SUPG}}$ , see Figures 5 and 6 for the case  $p = 3$ . In particular, as we can see in Figure 6,  $\tau_{\text{SUPG}} = \frac{h_t}{2}$  is the best value not only for  $p = 1$  (as presented in section 3.1) but also for high-degree splines.

Adding Shock Capturing with  $\tau_{\text{SC}} = h_t^2$  (Figure 7) spurious oscillations are reduced but present for any  $\tau_{\text{SC}}$  (Figure 8).

With the non consistent NCSU method (Figure 9) spurious oscillations disappear but the numerical and phase errors are significantly larger.



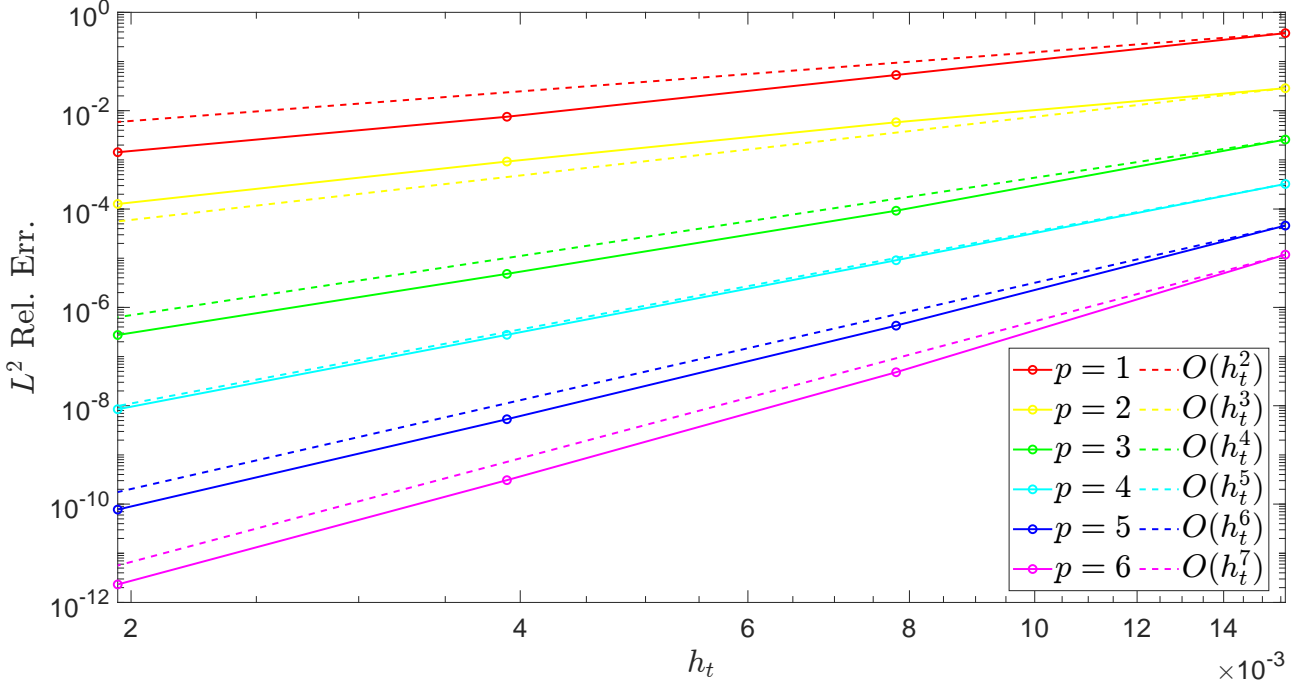


Figure 3: Advection equation, SU relative error plots in  $L^2$ -norm.

Figures 10 and 11 show numerical results for  $p = 3$  and  $p = 4$ , that assess the behavior of the SU formulation on uniform meshes: spurious oscillations are completely eliminated. Similar results are obtained from different degrees. Moreover relative error graphs in  $L^2$ -norm (Figure 12), calculated after the three layers where the solution is smooth ( $t > 0.85$ ), show that the relative error converges optimally.

Stable and accurate behavior of SU method is also confirmed if we deal with non-uniform meshes, as we can see in Figure 13.

## 5.2 Advection-diffusion equation

As in Section 5.1 we consider a uniform mesh. We consider the advection-diffusion equation (7) on  $(0, T)$  with  $T = 1$ ,  $f = 1$  and  $\varepsilon = 10^{-6}$ . Figures 14 and 15 show SUPG and SU solutions. The SU method demonstrates higher accuracy, albeit at a higher computational cost. In our implementation the increased cost arises from the need to evaluate the residual at each fixed point iteration. However, the issue of computational cost and efficient implementation deserves a more in-depth exploration beyond the scope of this work.

## 5.3 Heat equation

### 5.3.1 2D space-time domain

For the first test we consider  $\Omega = (0, 1)$ , we solve a uniform mesh and we use the same mesh-size in space and in time, i.e. we set  $h_s = h_t =: h$ . We consider the heat equation (8) on  $(0, 1) \times (0, T)$  with  $T = 1$  and  $f$  as follows:

$$f(x, t) = \delta^{-2} \exp(-((x - (1/4(\sin(10\pi t) + 2))))/\delta)^2) \chi_{[0.3, 0.6]}(t),$$

where

$$\chi_{[0.3, 0.6]}(t) = \begin{cases} 1 & \text{for } t \in [0.3, 0.6], \\ 0 & \text{otherwise,} \end{cases}$$

and with  $\delta = 10^{-3}$ .

In Figures 16, 17 and 18 the numerical solutions by Galerkin, SUPG and the SU methods are presented. Figure 19 displays the graph of the function  $\theta(x, t)$ , which plays a crucial role in activating the high-order Upwind stabilization in the proximity of the layers. The function  $\theta(x, t)$  serves as a key indicator, guiding the activation of the stabilization technique to effectively address the presence of sharp layers in the solution.

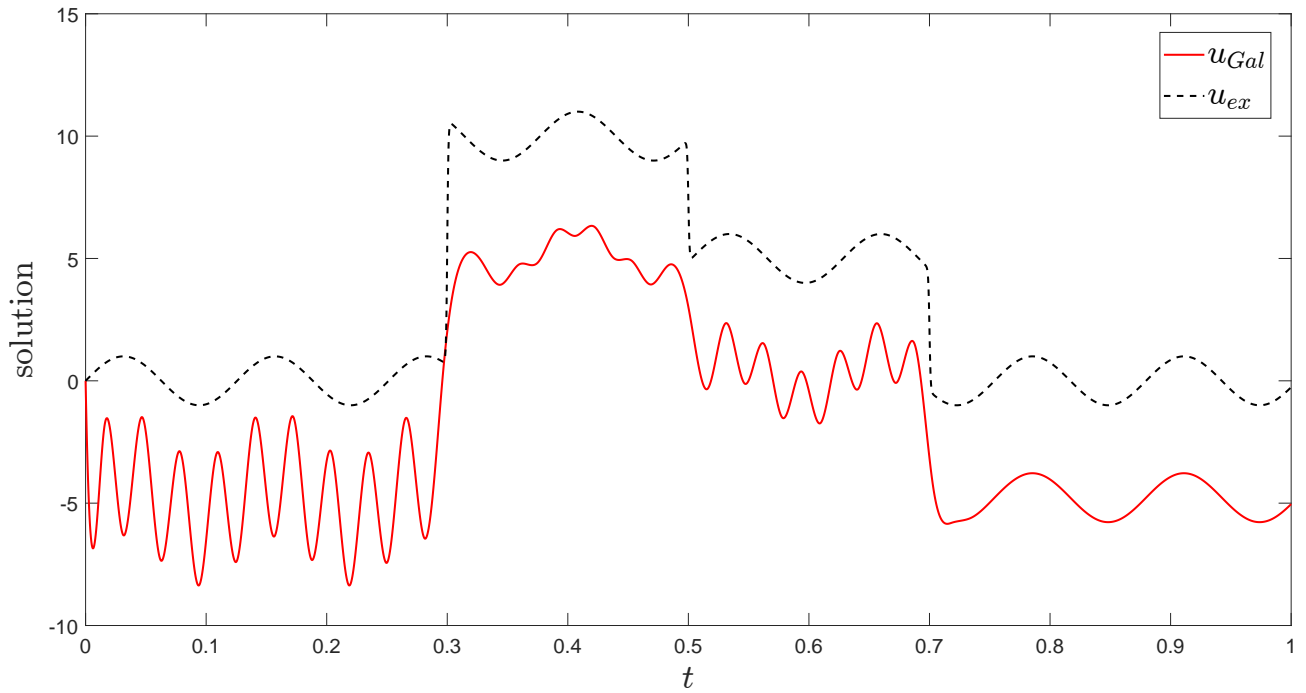


Figure 4: Advection equation, exact and standard Galerkin solutions, with  $h_t = 2^{-6}$  and  $p = 3$ .

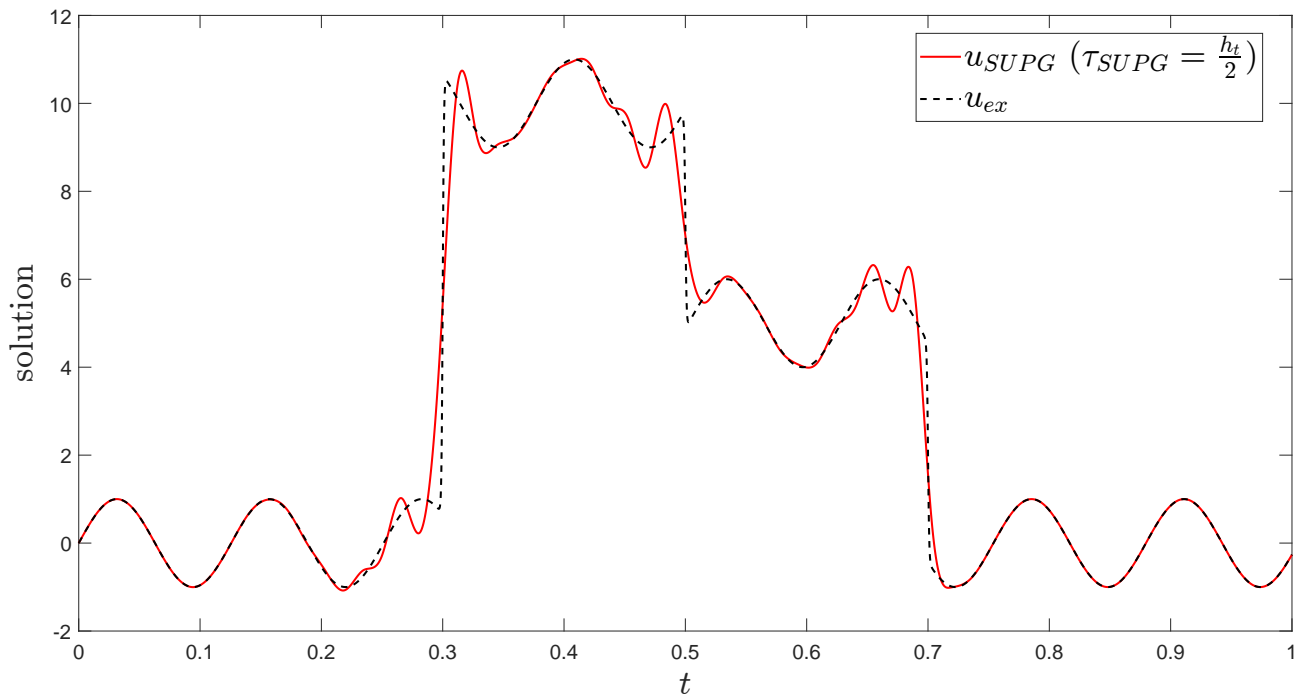


Figure 5: Advection equation, exact and SUPG solutions, with  $h_t = 2^{-6}$  and  $p = 3$ .

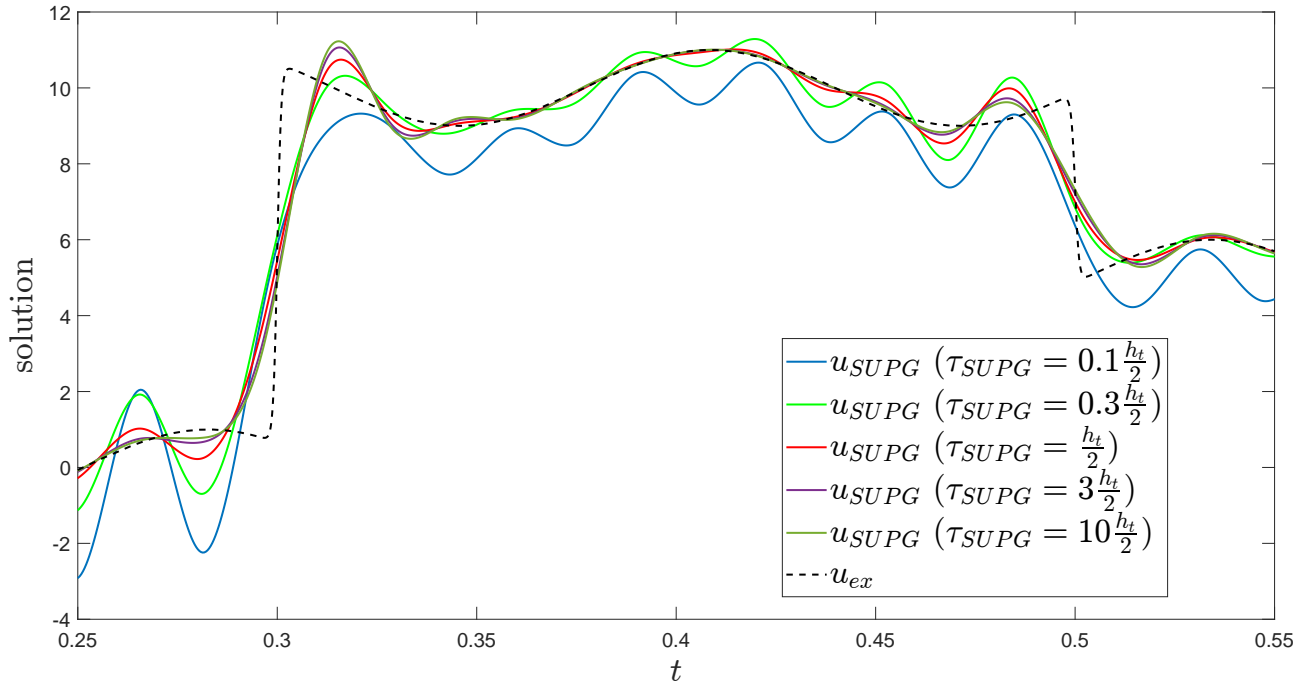


Figure 6: Advection equation, exact and SUPG solutions for different choices for  $\tau_{SUPG}$ , with  $h_t = 2^{-6}$  and  $p = 3$ .

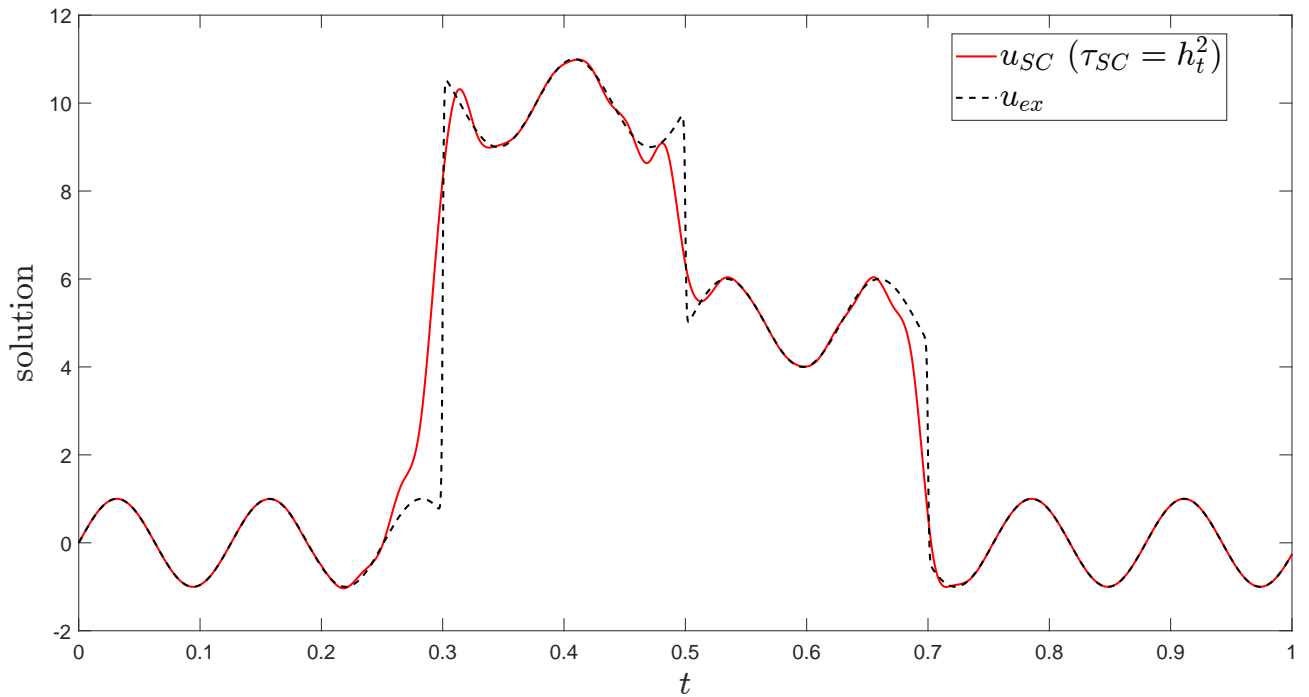


Figure 7: Advection equation, exact and Shock Capturing solutions, with  $h_t = 2^{-6}$  and  $p = 3$ .

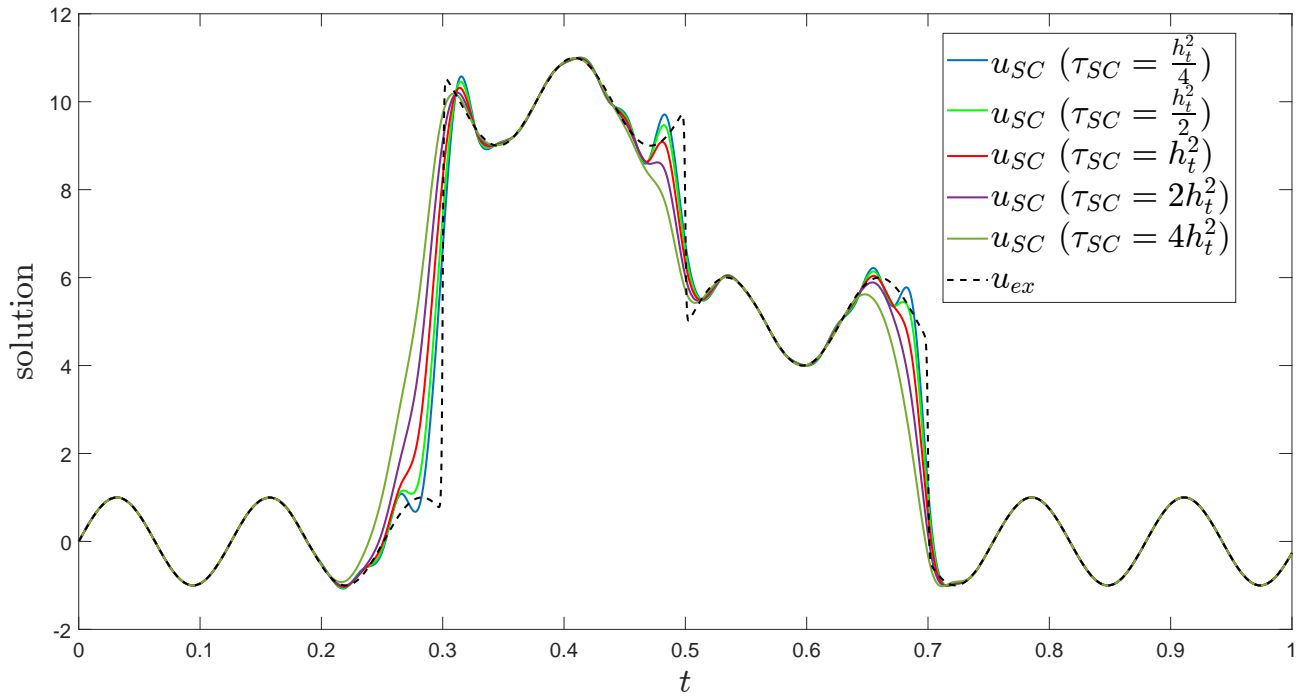


Figure 8: Advection equation, exact and Shock Capturing solutions for different choices for  $\tau_{SC}$ , with  $h_t = 2^{-6}$  and  $p = 3$ .

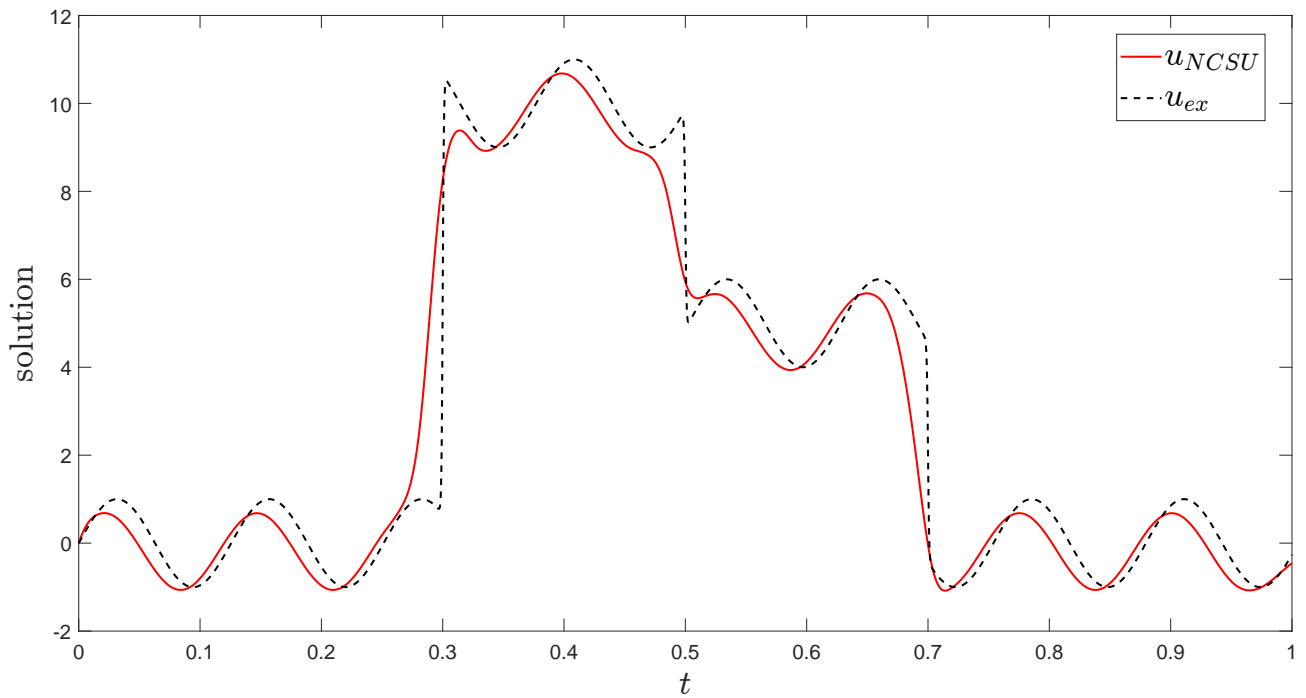


Figure 9: Advection equation, exact and NCSU solutions, with  $h_t = 2^{-6}$  and  $p = 3$ .

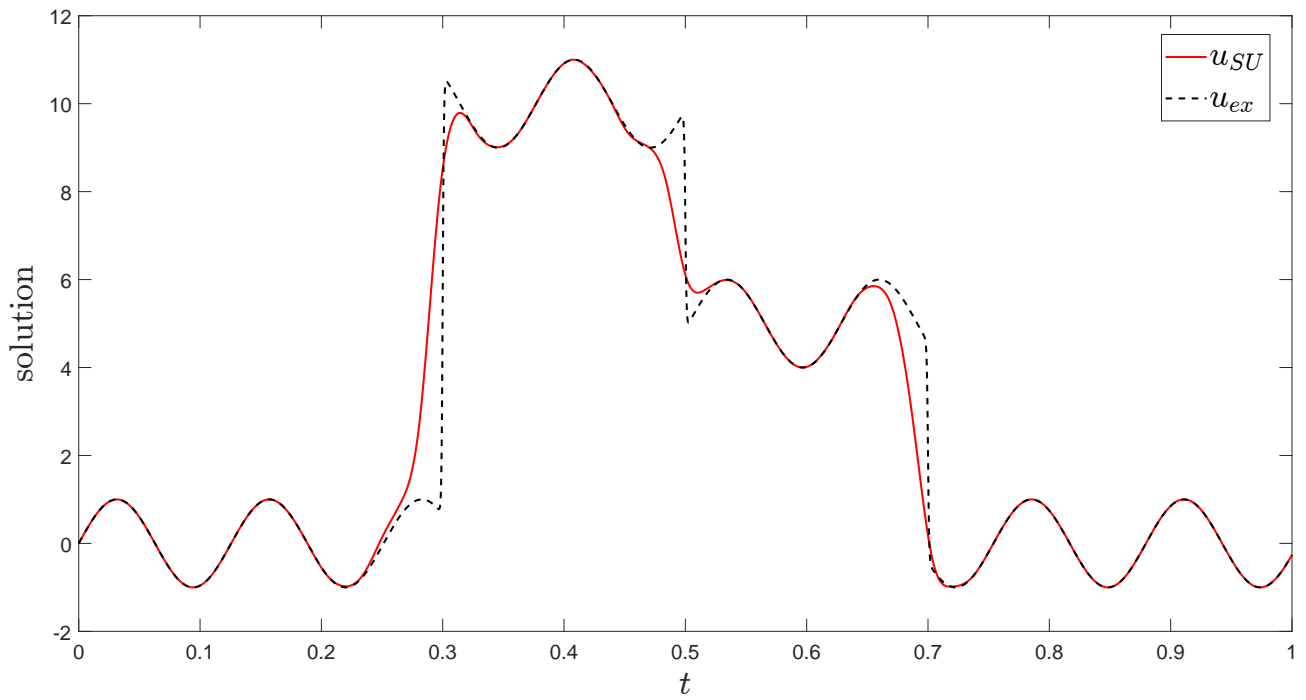


Figure 10: Advection equation, exact and SU solutions, with  $h_t = 2^{-6}$  and  $p = 3$ .

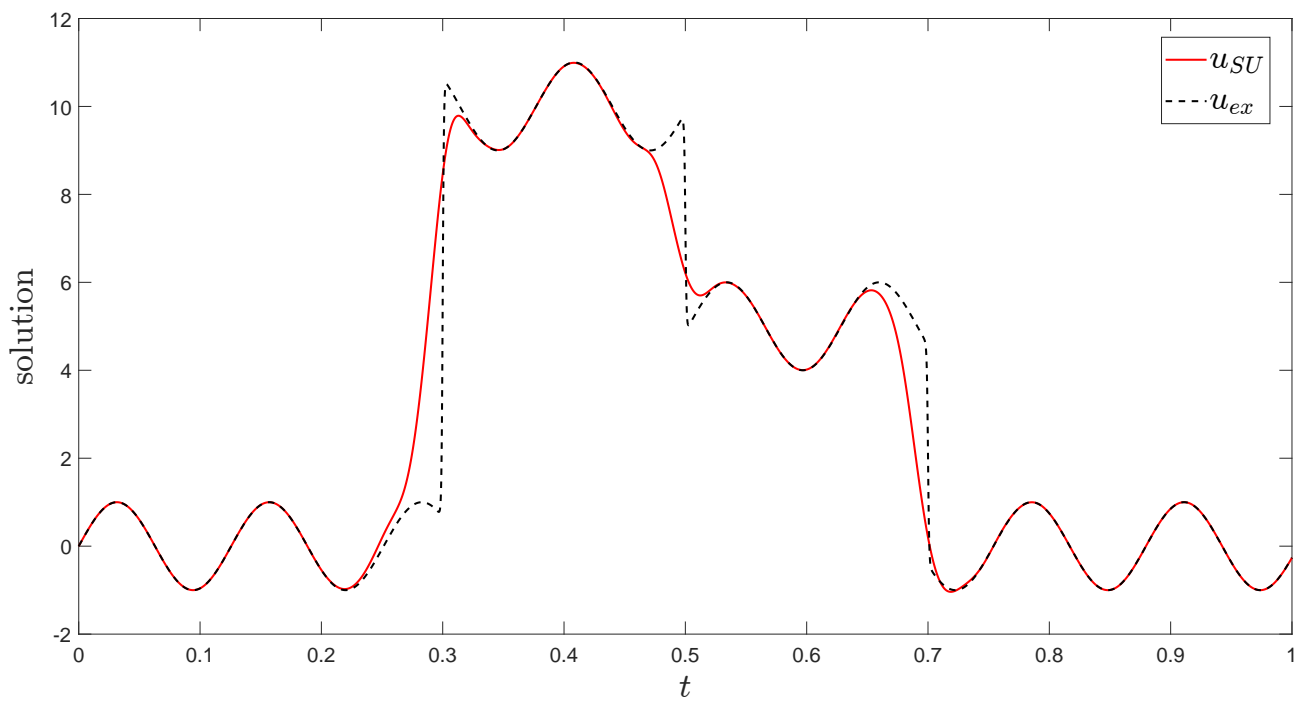


Figure 11: Advection equation, exact and SU solutions, with  $h_t = 2^{-6}$  and  $p = 4$ .

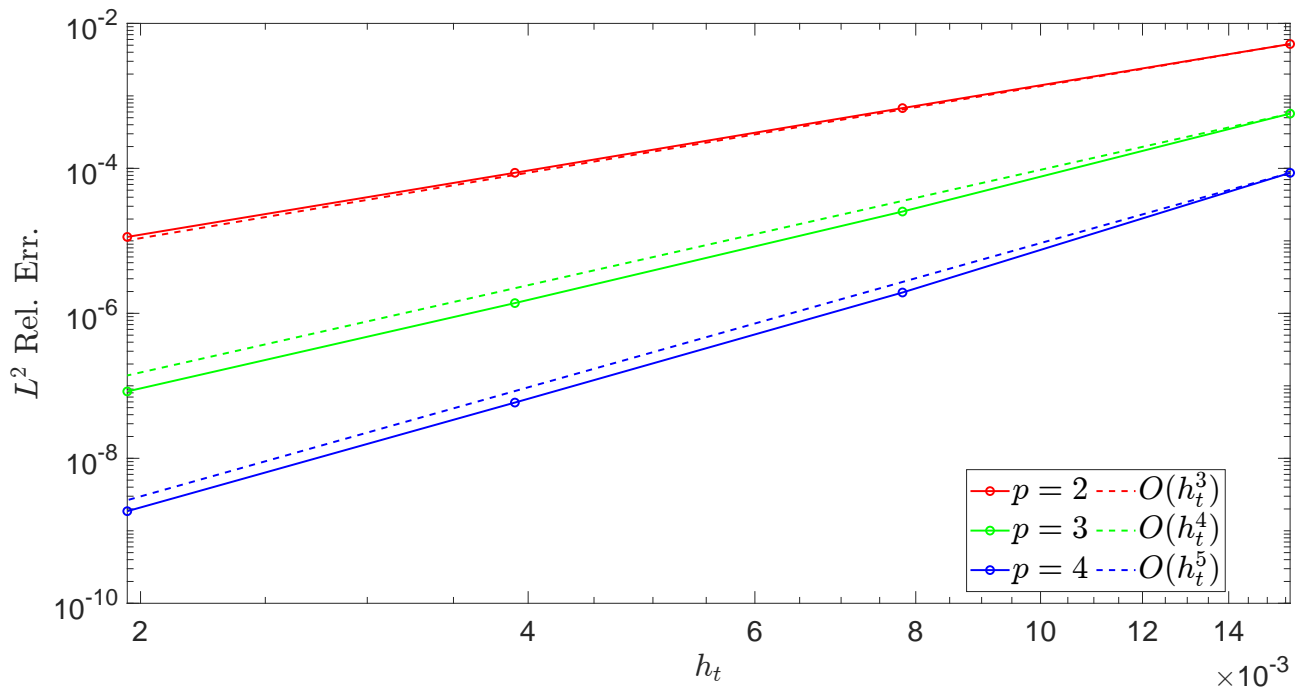


Figure 12: Advection equation, SU relative error plots in  $L^2$ -norm computed where the solution is smooth.

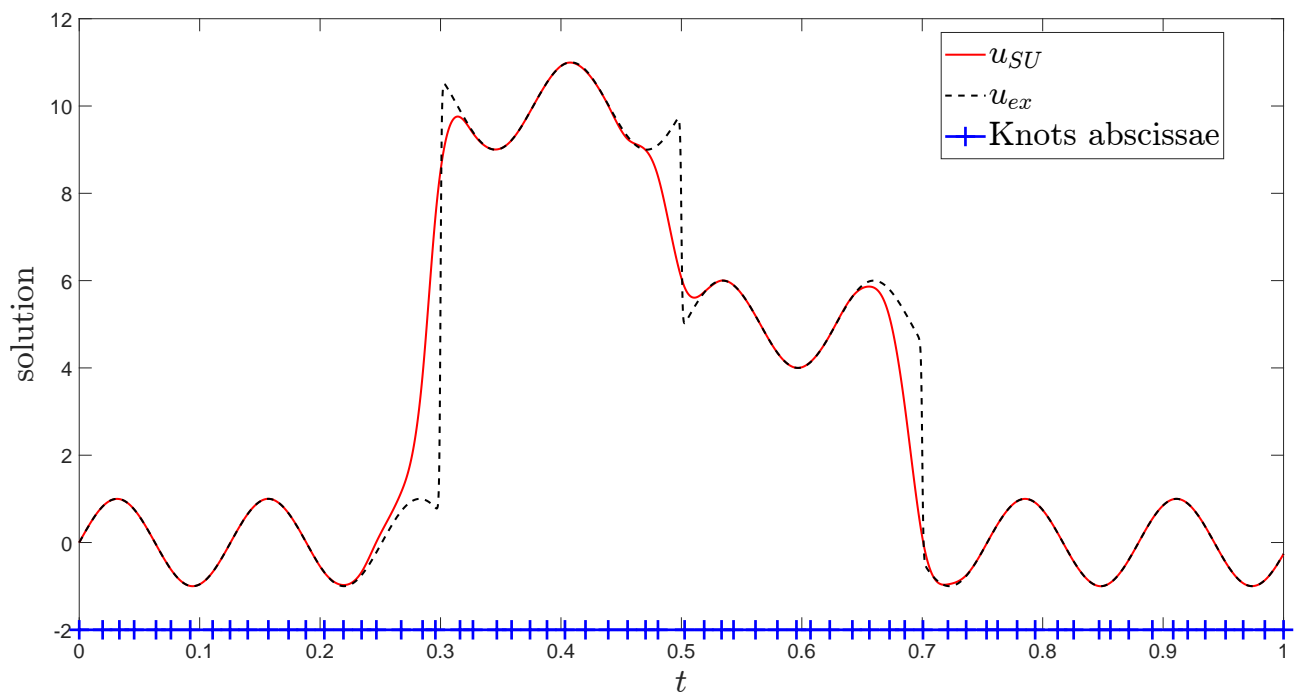


Figure 13: Advection equation, exact and SU solutions on a non-uniform mesh (depicted in blue on the horizontal axis) and  $p = 3$ .

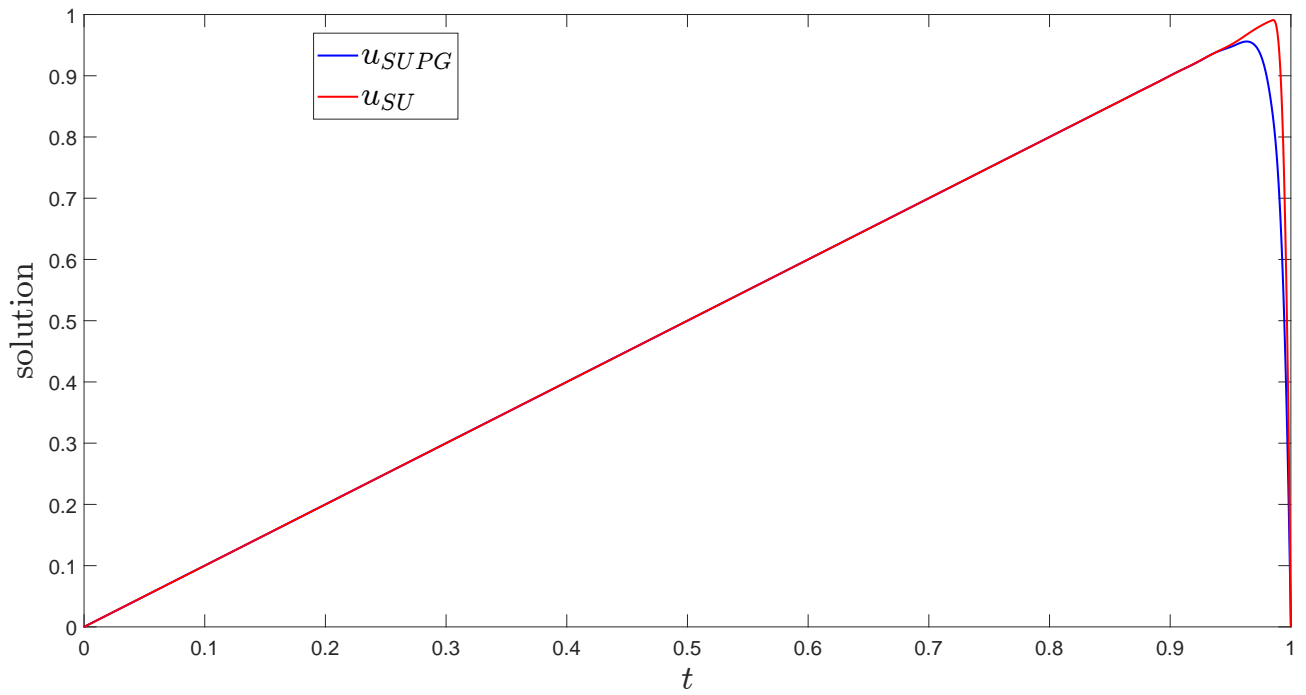


Figure 14: Advection-diffusion equation, SUPG and SU solution;  $h_t = 2^{-6}$  and  $p = 3$ .

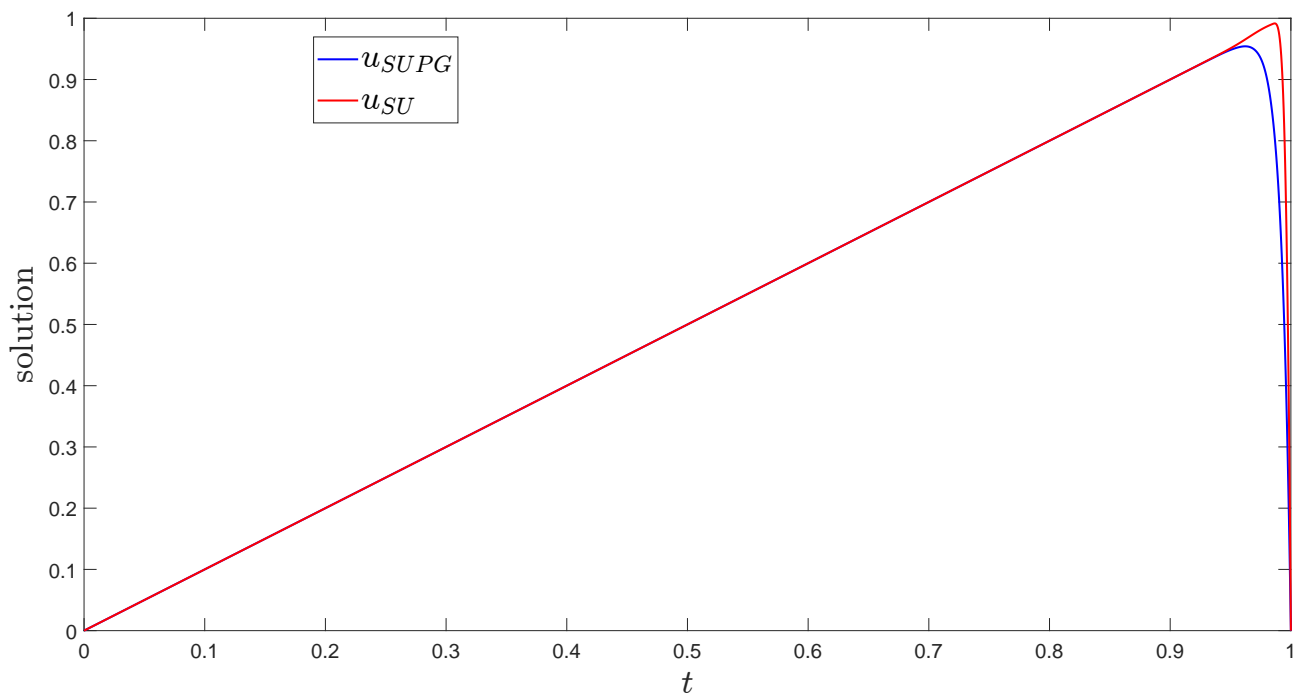


Figure 15: Advection-diffusion equation, SUPG and SU solution;  $h_t = 2^{-6}$  and  $p = 4$ .

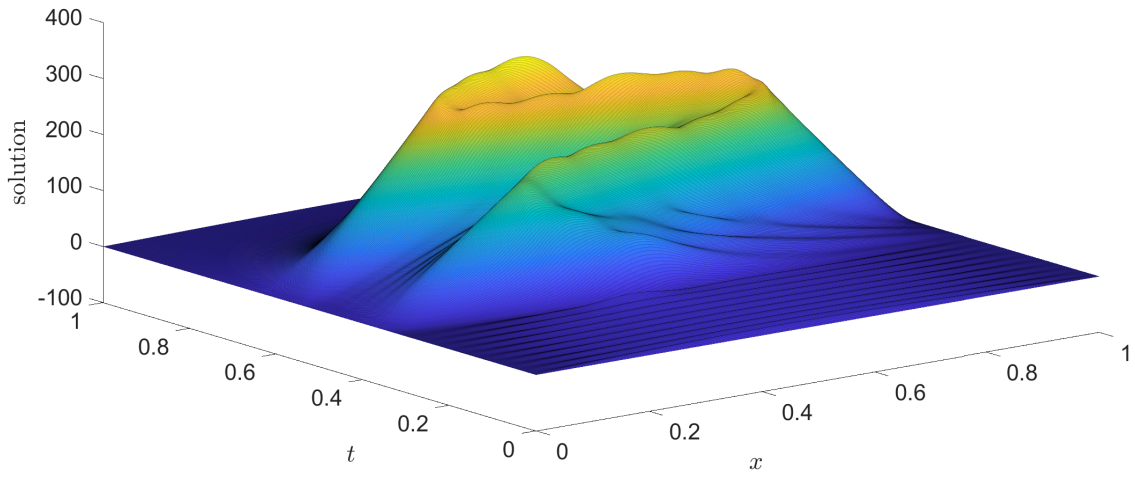


Figure 16: Numerical solution of the Galerkin method for the heat equation ( $\Omega = (0, 1)$ ), with  $h = 2^{-6}$  and  $p = 3$ , spurious oscillations are present also for  $t < 0.3$ .

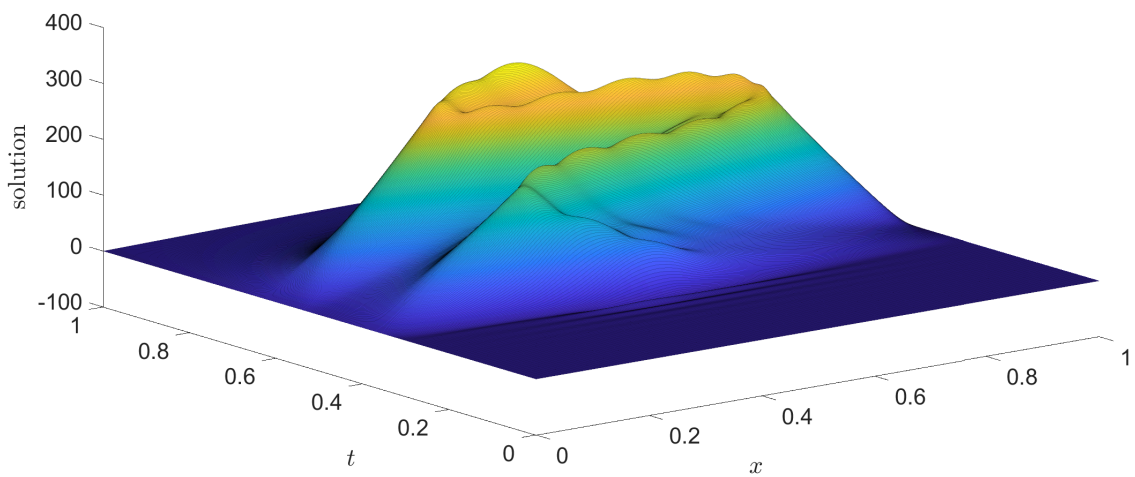


Figure 17: Numerical solution of SUPG method for the heat equation ( $\Omega = (0, 1)$ ), with  $h = 2^{-6}$  and  $p = 3$ .



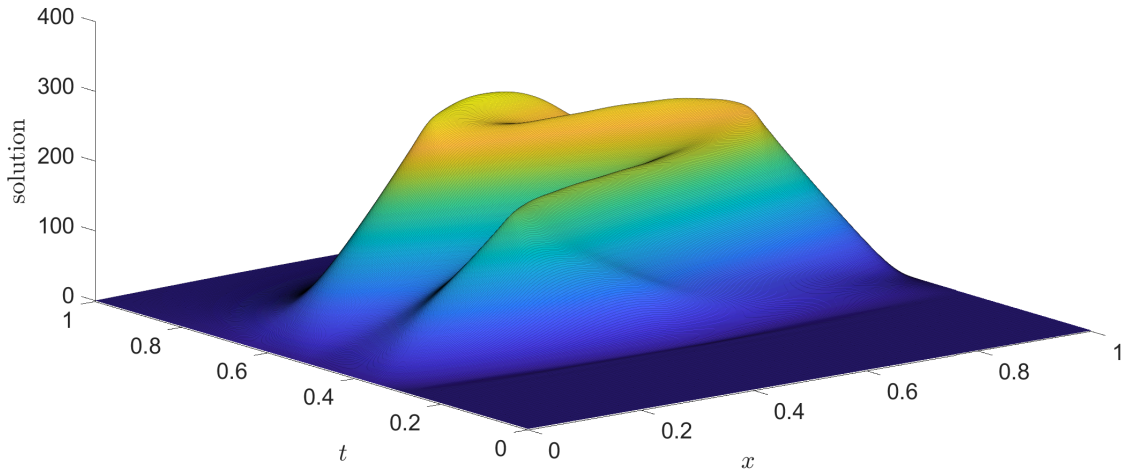


Figure 18: Numerical solution of the SU method for the heat equation ( $\Omega = (0, 1)$ ), with  $h = 2^{-6}$  and  $p = 3$ .

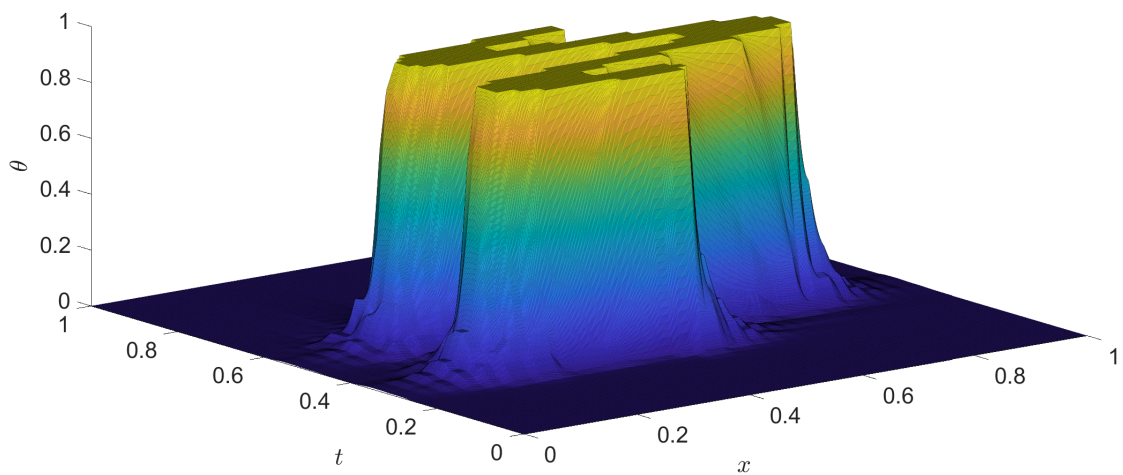


Figure 19: function  $\theta(x, t)$  ( $\Omega = (0, 1)$ ), with  $h = 2^{-6}$  and  $p = 3$ .

### 5.3.2 3D space-time domain

For the second test we take as  $\Omega$  a quarter annulus (Figure 20), and set

$$f(x_1, x_2, t) = 10^3 / (2\pi\delta^2) \exp(-1/2(((x_1 - 1.5 \cos(\pi/2t))/\delta)^2 + ((x_2 - 1.5 \sin(\pi/2t))/\delta)^2)) \chi_{[0.3, 0.6]}(t),$$

with  $\delta = 0.1$ .

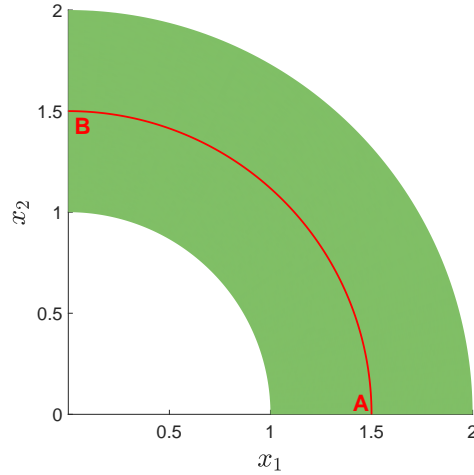


Figure 20: Quarter annulus with section line A-B.

In Figures 21 and 22 the numerical results that assess the behavior of the space-time Galerkin approximation and SUPG method are presented. As in Section 5.3.1, we observe the emergence of spurious oscillations, particularly in the case of the plain Galerkin method. However, when examining the numerical results of the SU method in Figure 23, we can see that they are free from spurious oscillations.

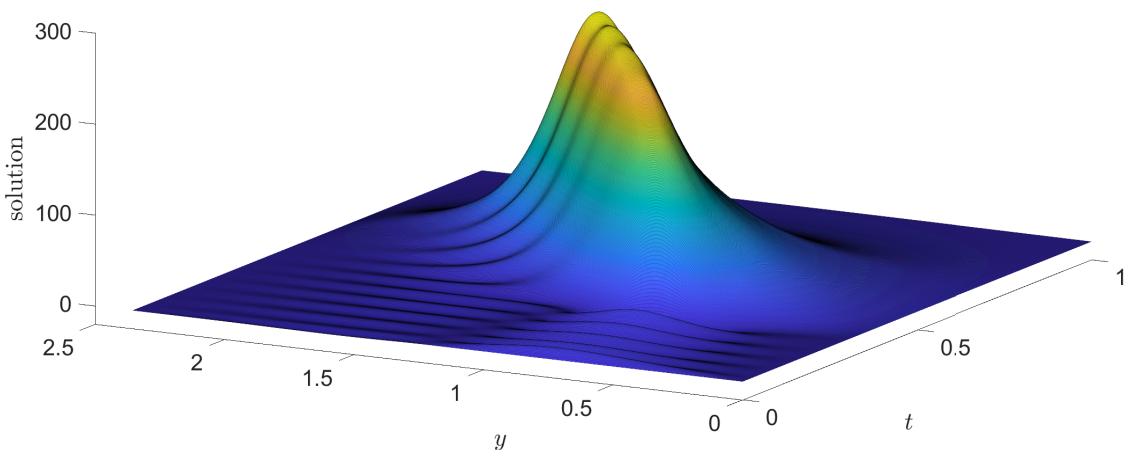


Figure 21: Numerical solution of Galerkin method (along section A-B) for the heat equation on the quarter annulus, with  $h = 2^{-5}$  and  $p = 3$ , spurious oscillations are present also for  $t < 0.3$ .

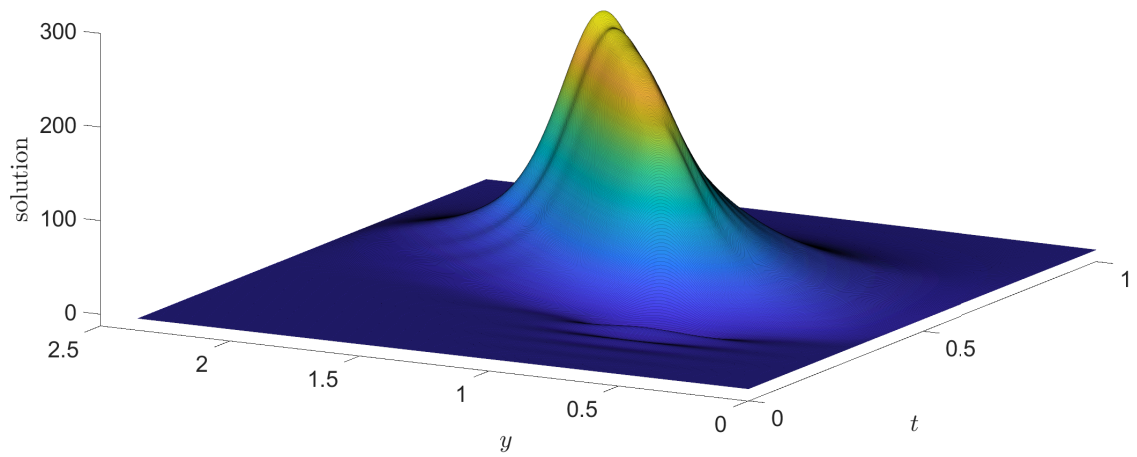


Figure 22: Numerical solution of SUPG method (along section A-B) for the heat equation on the quarter annulus, with  $h = 2^{-5}$  and  $p = 3$ .

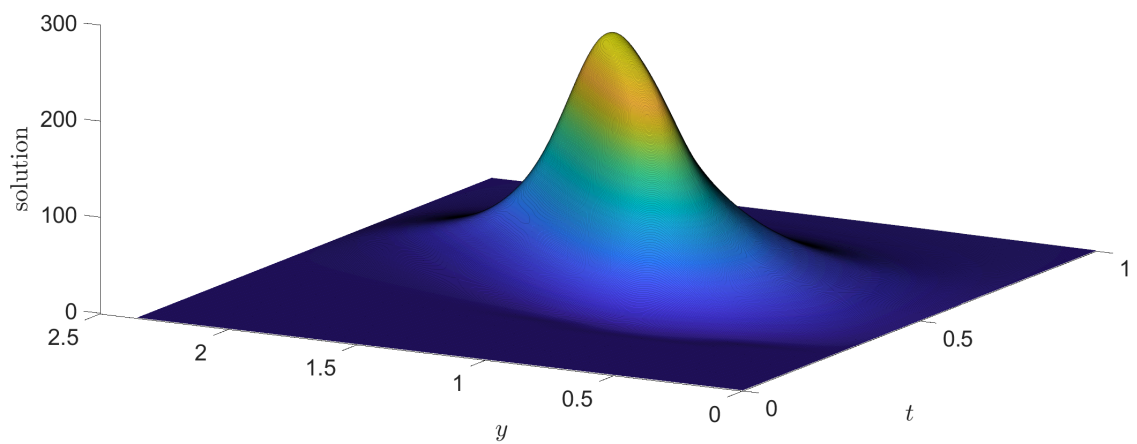


Figure 23: Numerical solution of the SU method (along section A-B) for the heat equation on the quarter annulus, with  $h = 2^{-5}$  and  $p = 3$ .

## 6 Conclusions

In this work, we have presented a novel space-time method for the heat equation in the framework of IgA. It is based on smooth spline approximation in time and incorporates a stabilizing term that extends the SUPG stabilization mechanism to high-degree and continuity splines, promoting causality with respect to time.

We have conducted various numerical benchmarks to validate our method. The results provided numerical evidence of the optimal order of convergence for smooth solutions and of the stable behavior even in the presence of sharp layers and concentrated source terms.

While our focus in this work was not on computational cost, we acknowledge the significance of efficient and fast solvers in the space-time framework. In particular the higher dimensionality poses computational challenges that need to be addressed. We plan to explore and address these computational aspects in future works.

## Acknowledgements

The authors are members of the Gruppo Nazionale Calcolo Scientifico-Istituto Nazionale di Alta Matematica (GNCS-INDAM). Support for this research was partially provided by a grant through Regione Lombardia, POR FESR 2014-2020 - Call HUB Ricerca e Innovazione, Progetto 1139857 CE4WE: Approvvigionamento energetico e gestione della risorsa idrica nell'ottica dell'Economia Circolare (Circular Economy for Water and Energy). G. Loli was also partially supported by the GNCS-INDAM through the "Bando Finanziamento Giovani Ricercatori 2021-2022 GNCS". The authors acknowledge the contribution of the National Recovery and Resilience Plan, Mission 4 Component 2 - Investment 1.4 - NATIONAL CENTER FOR HPC, BIG DATA AND QUANTUM COMPUTING, spoke 6.

## References

- [1] T. J. R. Hughes, J. A. Cottrell, Y. Bazilevs, Isogeometric analysis: CAD, finite elements, NURBS, exact geometry and mesh refinement, *Computer Methods in Applied Mechanics and Engineering* 194 (39) (2005) 4135–4195. doi:10.1016/j.cma.2004.10.008.
- [2] J. A. Cottrell, T. J. R. Hughes, Y. Bazilevs, *Isogeometric analysis: toward integration of CAD and FEA*, John Wiley & Sons, 2009.
- [3] J. A. Evans, Y. Bazilevs, I. Babuška, T. J. R. Hughes,  $n$ -widths, sup-infs, and optimality ratios for the  $k$ -version of the isogeometric finite element method, *Computer Methods in Applied Mechanics and Engineering* 198 (2009) 1726–1741. doi:10.1016/j.cma.2009.01.021.
- [4] A. Bressan, E. Sande, Approximation in FEM, DG and IGA: a theoretical comparison, *Numerische Mathematik* 143 (4) (2019) 923–942. doi:10.1007/s00211-019-01063-5.
- [5] I. Fried, Finite-element analysis of time-dependent phenomena, *AIAA Journal* 7 (6) (1969) 1170–1173. doi:10.2514/3.5299.
- [6] J. T. Oden, A general theory of finite elements. II. Applications, *International Journal for Numerical Methods in Engineering* 1 (3) (1969) 247–259. doi:10.1002/nme.1620010304.
- [7] J. H. Argyris, D. W. Scharpf, Finite elements in time and space, *Nuclear Engineering and Design* 10 (4) (1969) 456–464. doi:10.1016/0029-5493(69)90081-8.
- [8] J. C. Bruch Jr., G. Zyzoloski, Transient two-dimensional heat conduction problems solved by the finite element method, *International Journal for Numerical Methods in Engineering* 8 (3) (1974) 481–494. doi:10.1002/nme.1620080304.
- [9] H. Nguyen, J. Reynen, A space-time least-square finite element scheme for advection-diffusion equations, *Computer Methods in Applied Mechanics and Engineering* 42 (3) (1984) 331–342. doi:10.1016/0045-7825(84)90012-4.
- [10] T. J. R. Hughes, G. M. H. Hulbert, Space-time finite element methods for elastodynamics: Formulations and error estimates, *Computer Methods in Applied Mechanics and Engineering* 66 (3) (1988) 339–363. doi:10.1016/0045-7825(88)90006-0.

- [11] C. Schwab, R. Stevenson, Space-time adaptive wavelet methods for parabolic evolution problems, *Mathematics of Computation* 78 (267) (2009) 1293–1318. doi:10.1090/S0025-5718-08-02205-9.
- [12] O. Steinbach, Space-Time Finite Element Methods for Parabolic Problems, *Computational Methods in Applied Mathematics* 15 (4) (2015) 551–566. doi:10.1515/cmam-2015-0026.
- [13] K. Takizawa, T. Tezduyar, Space-time computation techniques with continuous representation in time (ST-C), *Computational Mechanics* 53 (1) (2014) 91–99. doi:10.1007/s00466-013-0895-y.
- [14] U. Langer, S. E. Moore, M. Neumüller, Space-time isogeometric analysis of parabolic evolution problems, *Computer Methods in Applied Mechanics and Engineering* 306 (2016) 342 – 363. doi:10.1016/j.cma.2016.03.042.
- [15] M. Montardini, M. Negri, G. Sangalli, M. Tani, Space-time least-squares isogeometric method and efficient solver for parabolic problems, *Mathematics of Computation* 89 (323) (2020) 1193–1227. doi:10.1090/mcom/3471.
- [16] G. Loli, M. Montardini, G. Sangalli, M. Tani, An efficient solver for space-time isogeometric Galerkin methods for parabolic problems, *Computers and Mathematics with Applications* 80 (11) (2020) 2586–2603. doi:10.1016/j.camwa.2020.09.014.
- [17] C. Saadé, S. Lejeunes, D. Eyheramendy, R. Saad, Space-Time Isogeometric Analysis for linear and non-linear elastodynamics, *Computers & Structures* 254 (2021) 106594. doi:10.1016/j.compstruc.2021.106594.
- [18] A. N. Brooks, T. J. R. Hughes, Streamline upwind/Petrov-Galerkin formulations for convection dominated flows with particular emphasis on the incompressible Navier-Stokes equations, *Computer Methods in Applied Mechanics and Engineering* 32 (1) (1982) 199–259. doi:10.1016/0045-7825(82)90071-8.
- [19] P. Kopp, V. Calo, E. Rank, S. Kollmannsberger, Space-time hp-finite elements for heat evolution in laser powder bed fusion additive manufacturing, *Engineering with Computers* 38 (6) (2022) 4879–4893. doi:10.1007/s00366-022-01719-1.
- [20] U. Langer, O. Steinbach, F. Troltzsch, H. Yang, Unstructured space-time finite element methods for optimal control of parabolic equations, *SIAM Journal on Scientific Computing* 43 (2) (2021) A744–A771. doi:10.1137/20M1330452.
- [21] M. J. Gander, 50 years of time parallel time integration, in: T. Carraro, M. Geiger, S. Körkel, R. Rannacher (Eds.), *Multiple Shooting and Time Domain Decomposition Methods*, Springer International Publishing, Cham, 2015, pp. 69–113. doi:10.1007/978-3-319-23321-5.
- [22] U. Langer, O. Steinbach, *Space-Time Methods: Applications to Partial Differential Equations*, Vol. 25, Walter de Gruyter GmbH & Co KG, 2019. doi:10.1515/9783110548488.
- [23] Y. Bazilevs, V. M. Calo, T. E. Tezduyar, T. J. R. Hughes,  $YZ\beta$  discontinuity capturing for advection-dominated processes with application to arterial drug delivery, *International Journal for Numerical Methods in Fluids* 54 (6-8) (2007) 593–608. doi:10.1002/flid.1484.
- [24] R. Vázquez, A new design for the implementation of isogeometric analysis in Octave and Matlab: GeoPDEs 3.0, *Computers & Mathematics with Applications* 72 (3) (2016) 523–554. doi:10.1016/j.camwa.2016.05.010.